THE JOURNAL OF PHYSICAL CHEMISTRY C

ARTICLE

pubs.acs.org/JPCC

Origin of Photocatalytic Activation of Silver Orthophosphate from First-Principles

Xinguo Ma, Bin Lu, Di Li, Rui Shi, Chenshi Pan, and Yongfa Zhu*

Department of Chemistry, Tsinghua University, Beijing 100084, PR China

Supporting Information

ABSTRACT: First-principles density functional theory incorporating the LDA + U formalism has been used to investigate the origin of photocatalytic activation of Ag_3PO_4. The approach provides an improved band gap and the position of the valence band if both U_p and U_d are used. Through examining the energy band structure and density of states, we can understand why Ag_3PO_4 is a promising photocatalyst for oxidizing water as well as degrading organic contaminants. The results show that Ag_3PO_4 has a large dispersion of conduction band and the inductive effect of PO_4^{3-}, which help the separation of electron−hole pairs. It is demonstrated theoretically that Ag vacancies in Ag_3PO_4 with high concentration have a significant effect on the separation of electron−hole pairs and optical absorbance in the visible-light region. These findings present a reasonable explanation of recent experimental results.

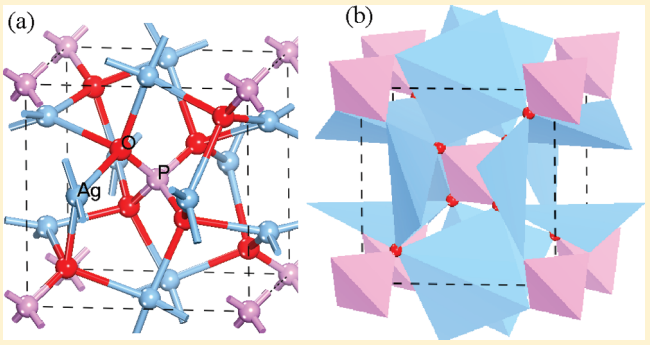

1. INTRODUCTION

An intense research activity has been recently devoted to search for active semiconductor photocatalysts that directly split water or degrade environmental pollutants under sunlight irradiation. Both strong light absorption and suitable redox potential are prerequisites for photocatalytic reaction. Unfortunately, at present, most semiconductors cannot meet all the criteria. TiO_2 has been used as a photocatalyst because of its high activation, long-term stability, low price, and availability, but its band gap is too wide to absorb sunlight efficiently. In the recent years, a growing interest was also focused on the non-TiO_2-based catalyzers, such as $InMO_4$ (M = Nb, Ta),[1] $BiVO_4$,[2,3] Bi_2WO_6,[4,5] $Ga_{1-x}Zn_xN_{1-x}O_x$,[6,7] Ag_2CrO_4,[8] and so on; however, the present achievements are still far from the ideal goal. Recently, Yi et al. found a new use for the silver orthophosphate (Ag_3PO_4) semiconductor, which can harness visible light to oxidize water as well as degrade organic contaminants in aqueous solution.[9] It was found that the process of methylene blue decomposition over Ag_3PO_4 was dozens of times quicker than that over monoclinic $BiVO_4$ and commercial $TiO_{2-x}N_x$. This suggests its potential as a photofunctional material for wastewater cleaning.

Ag_3PO_4 has been the subject of several experimental investigations. Most of the works are devoted to the synthesizing and characterization of its polymorphs.[10,11] The accurate crystal structure involving the determination of the silver and phosphorus fractional coordinates was established.[9−11] The strong photooxidation of the Ag_3PO_4 semiconductor stimulates us to explore its application as a photocatalyst. However, the origin of photocatalytic activation still is not understood. Thus, accurate calculations of the geometry structure and electronic structure of Ag_3PO_4 are necessary to explore why Ag_3PO_4 is a promising photocatalyst for oxidizing water as well as degrading organic contaminants.

In the past decade, many theoretical investigations employed the local density approximation (LDA)[12] and the generalized gradient approximation (GGA)[13] to calculate the electronic structure of wide band gap transition metal oxides. However, they fail to give even reasonably accurate results for their band characteristics and especially band gap values.[14] These approaches underestimate the binding energy of the semicore d states and consequently overestimate their hybridization with the anion p-derived valence states, enhancing the effects of the p−d coupling. The artificially large p−d coupling pushes up the valence band maximum (VBM), leading to a reduction in the calculated band gap. The LDA + U approach aims to correct for this by adding an orbital-dependent term to the LDA potential. This is true for the highly correlated systems exhibiting strong effective on-site Coulomb interactions (U) between localized elections. Previous LDA + U studies did point to the fact that the band gap of transition metal oxide strongly depends on the Hubbard U parameters.[15] When the correction is only applied on transition metal d orbitals, however, the band gap value is still underestimated compared to the experimental band gap, even at high U values.[16−18] Recently, a few theoretical studies on transition metal oxides discussed the effect of U parameter on the p electrons (U_p) of oxygen in addition to the d electrons (U_d) of transition metal.[17−20]

Received: November 23, 2010
Revised: February 10, 2011
Published: February 25, 2011

Table 1. Structure Parameters of Ag_3PO_4: Lattice Parameters and Atom Positions[a]

			bond length/Å		bond angle (deg)			fractional coordinates		
method	a/Å	E_g/eV	P−O	Ag−O	O−P−O	O−Ag−O		x	y	z
expt.[b]	6.004	2.36	1.539	2.345	109.470	93.660	Ag	0.231	0	0.500
			1.539	2.403			P	0	0	0
							O	0.148	0.148	0.148
GGA-PBE	6.113	0.30	1.549	2.364	109.307	92.994	Ag	0.231	0	0.501
			1.557	2.400			P	0	0	0
							O	0.146	0.146	0.146
LDA-CAPZ	5.890	0.46	1.529	2.314	109.471	93.688	Ag	0.250	0	0.500
			1.529	2.414			P	0	0	0
							O	0.150	0.150	0.150

[a] E_g denotes band gap energy. [b] Ref 10.

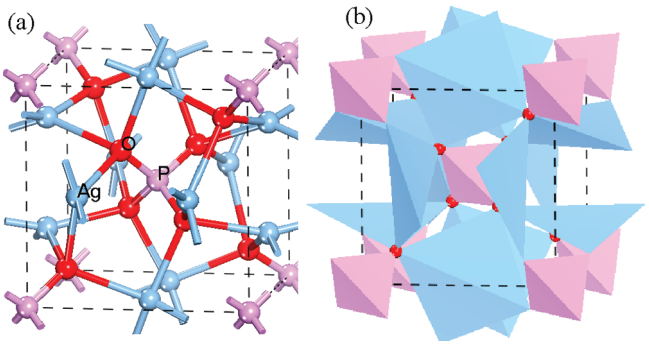

Figure 1. Unit-cell structure of cubic Ag_3PO_4, showing (a) ball and stick and (b) polyhedron configurations. Red, purple, and blue spheres represent O, P, and Ag atoms, respectively.

In this work, we present the calculated results of electronic properties of Ag_3PO_4 using first-principles density functional theory (DFT) incorporating the LDA + U formalism, where the parameter U is applied on the 4d orbital electrons of Ag atoms and p orbital electrons of the O and P atoms. Here, the absolute energy positions of conduction band (CB) and valence band (VB) edges are compiled for Ag_3PO_4 based on experiment data and complementary empirical calculations from electronegativities of constituent elements. We also discuss the effective mass of the charge carrier. Finally, the formation energies of Ag vacancies in Ag_3PO_4 are calculated, and the defect states of Ag vacancies are discussed.

2. CALCULATION METHODS

The theoretical calculations were performed using the plane-wave pseudopotential DFT method as implemented in the CASTEP code.[21] The LDA and GGA are used to describe the exchange and correlation energy of the electrons.[12,13] The ion−electron interaction is modeled by ultrasoft pseudopential in the Vanderbilt form.[22] The valence atomic configurations are $2s^22p^4$ for O, $3s^23p^3$ for P, and $4d^{10}5s^1$ for Ag, respectively. The energy cutoff for a plane wave basis set is 400 eV, and a Monkhorst−Pack k-mesh of 6 × 6 × 6 is used.[23] To find the optimum U_d and U_p parameters, we applied various values of U_d and U_p to investigate their effect on the energy band structure of Ag_3PO_4. Geometry optimizations are done before single-point energy calculation, and the self-consistent convergence accuracy is set at 1×10^{-6} eV/atom. The convergence criterion for the maximal force between atoms is 0.01 eV. The maximum displacement is 5×10^{-4} Å, and the stress is 0.02 GPa. The Mulliken charge and bond population are investigated using a projection of the plane-wave states onto a linear combination of the atomic orbital (LCAO) basis set,[24,25] which is widely used to perform charge transfers and population analyses. Due to complete symmetry between spin-up and spin-down states, we only showed the spin-up results in this paper.

3. RESULTS AND DISCUSSION

3.1. Geometry Structure and Mulliken Population. Ag_3PO_4 is known to crystallize in the cubic structure with space group $P4\text{-}3n$ (NO. 218). The crystal structure determined by XRD using Cu Kα radiation consists of isolated, regular PO_4 tetrahedra forming a body-centered cubic lattice.[10,11] The six Ag atoms in the present case are assigned the 12(h) positions. This means that each Ag atom at (0.25, 0, 0.50) actually occupies one of the two sites at (x, 0, 0.50) and (0.5 − x, 0, 0.50) on the 2-fold axis.[10] As shown in Figure 1, the Ag atom experiences 4-fold coordination by four O atoms. The P atoms have 4-fold coordination surrounded by four O atoms, while the O atoms have 4-fold coordination surrounded by three Ag atoms and one P atom. By minimizing the crystal total energy, the equilibrium lattice parameters have been calculated using LDA and GGA methods, and the results are given in Table 1 with the experimental values.[10] The former approximation, LDA, underestimates the lattice constant and overestimates cohesive energies relative to the experimental values, while the opposite is true for GGA. Our calculated equilibrium structural parameters are in very good agreement with experimental values within deviations of 2% in the lattice constants.

As for the chemical bonding behavior in Ag_3PO_4, we simply performed the corresponding atomic Mulliken charge and overlap population to analyze the bonding character quantitatively. The calculated results are given in Table 2. The Mulliken charges transferring from Ag and P to O atoms are 0.45e and 2.13e, respectively, so each O atom averagely obtains 0.87e. The Mulliken charges of Ag and O atoms in Ag_3PO_4 are larger than that in Ag_2O,[26] due to the incorporation of P atoms yielding the stable PO_4 tetrahedron configurations. Table 2 also shows the overlap populations for nearest neighbors in the crystal. Positive and negative values indicate bonding and antibonding states, respectively, and a value close to zero indicates that there is no significant interaction between the two atoms.[25,27] The overlap population between P and O atoms is 0.63e, and the bonding shows the covalent nature. However, the Ag−O bond shows a little of the covalent nature

dx.doi.org/10.1021/jp111167u |J. Phys. Chem. C 2011, 115, 4680–4687

Table 2. Atomic Mulliken Charge (e) and Overlap Population (eV) of Ag_3PO_4 by LDA and LDA + U_d + U_p[a]

species	s	p	d	total	charge	bonds	length/Å	population
Ag	0.34	0.33	9.88	10.55	0.45(0.54)	P−O	1.529	0.63(0.66)
P	0.90	1.96	0.00	2.87	2.13(2.18)	Ag−O	2.314	0.16(0.19)
O	1.85	5.03	0.00	6.87	−0.87(−0.95)	O−O	2.498	−0.13(−0.13)
						Ag−Ag	2.940	−0.04(−0.04)

[a] The values in brackets correspond to $U_{p,P} = U_{p,O} = 7$ eV and $U_{d,Ag} = 7.2$ eV.

whose overlap population is 0.16e. It is indicated that the covalency between P and O atoms is greater than that between Ag and O atoms, which could affect the band edge positions of Ag_3PO_4. We also found that by applying both U_d and U_p the Mulliken charge on each Ag and P atom is reduced by about 0.09e and 0.05e, respectively, while that on each O atom is increased by about 0.08e, indicating that the LDA + U approach predicts a more ionic bond character. There is an obvious directional bonding between P and O atoms and a litter of directional bonding between Ag and O atoms (see Figure S1 of the Supporting Information).

Figure 1(b) shows that the polyhedron configuration of Ag_3PO_4 consists of tetrahedral PO_4 and AgO_4. It is obvious that one PO_4 tetrahedron and three tetrahedral AgO_4 are combined with each other through the corner oxygen. The tetrahedral AgO_4 are heavily distorted to have a dipole moment of 2.2 D (D = debye), which should be closely attributed to a specific nonmetal salt of the oxy-acid structure of Ag_3PO_4. It is noteworthy that PO_4^{3-} ions have a large negative charge which maintains a large dipole in the Ag_3PO_4, which results in the distortion of tetrahedral AgO_4. This effect is called an inductive effect described as the action of one group affecting electrostatically the electron distribution in another group.[28,29] This effect may also be seen in other phosphate salts like $LiFePO_4$, in which the large negative charge of PO_4^{3-} ions is regarded to stabilize the Fe^{2+}/Fe^{3+}, so $LiFePO_4$ becomes a popular positive electrode material for lithium batteries.[28] Thus, a correlation between the photocatalytic activity and the distortion of AgO_4 tetrahedron is true for a specific phosphate structure. In the previous work, Inoue et al. show that $CaIn_2O_4$ and $SrIn_2O_4$ with a large dipole moment have a remarkable photocatalytic activity, while the negligible activity has been found on $LiInO_2$ and $NaInO_2$ with low local polarization.[29,30] Meanwhile, PO_4^{3-} possessing a large electron cloud overlapping (see Figure S1(a) of the Supporting Information) prefers to attract holes and repel electrons, which helps the e^-/h^+ separation.

3.2. Electronic Structure: LDA + *U* Description. The energy band structure and density of states (DOS) spectra of Ag_3PO_4 were calculated by LDA (see Figure S2 of the Supporting Information). A minimum direct band gap of about 0.38 eV was found at the Gamma-point (G). However, the energy difference in the VBM at G and Q points is only 0.08 eV. In other words, the plane-wave pseudopotential calculations yield an indirect transition from the VB at Q to the CB at G as the minimum band gap. The indirect band gap value of 0.30 eV obtained by LDA is 2.06 eV smaller than the experimental value previously reported by Yi et al.,[9] due to well-known limitations in DFT. In general, the energy for the transition metal d states within the LDA and GGA is too high, which results in their overhybridization with the p(O) states from the top of the VB. The use of the LDA + U approach would decrease both hybridization and the energy of the top of the VB.[20]

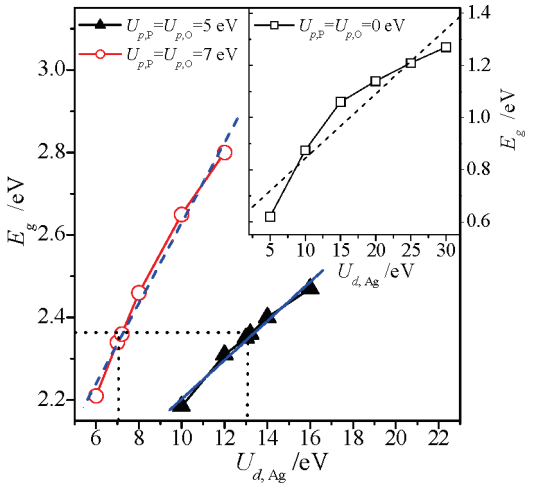

Figure 2. Band gap energy E_g as a function of U_d parameter within LDA + U_d + U_p and LDA + U_d (see the inset) approach. The corresponding experimental band gap is indicated by dashed lines.[9]

In most LDA + U studies for metal oxides, the U_d values were fitted in an empirical way.[18] To investigate the effect of U for Ag 4d, O 2p, and P 3p orbital electrons, we employed several calculations, in which a range of U_d and U_p values was chosen. If the U is incorporated only for the d states, the band gap energies are increased with increasing U_d values from 5 to 30 eV, from a value for 0.67 eV within the conventional LDA to 1.27 eV within LDA + U_d; however, the band gap energies are still underestimated compared to the experimental value of 2.36 eV (see inset of Figure 2). These indicate that the LDA + U_d approach may not be adequate to calculate the electronic structure of Ag_3PO_4. A corrected band gap energy can be obtained, however, if in addition to the U values for d states U values are included for the p states as well.[17,19] This raises an interesting question regarding the predictive ability of the LDA + U approach used in this work, in which the U value is required to be determined empirically through fitting to experimental data. In fact, different ways of determining U or the form of the localized orbitals can impact the results of a LDA + U calculation. With this in view, we performed extensive tests to determine the appropriate U parameters for Ag 4d, P 3p, and O 2p states to reproduce the corrected energy for the Ag 4d DOS peak and corrected band gap energy in Ag_3PO_4. Figure 2 also shows the relation between the band gap energy E_g and U values corresponding to LDA + U_d + U_p calculations, and where $U_{p,P}$ and $U_{p,O}$ are simultaneously fixed to 5 or 7 eV, the U_d ranges from 6 to 16 eV. The results show that the band gap energies are increased with increasing U_d values, where the optimum U_d value is 13.2 or 7.2 eV if $U_{p,P}$ and $U_{p,O}$ are simultaneously 5 or 7 eV, respectively. We noted that to describe consistently electronic structures in Al-doped SiO_2 and Li-doped MgO[31,32] a $U_{p,O}$ value of 7 eV is sufficient. This suggests that the description of O 2p states is independent of oxide material. More importantly, there exist experimental data in which the U_{p-p} for O 2p states has been determined. Auger spectroscopy studies of different oxides demonstrate that the on-site Coulomb interaction energy for a hole in an O 2p orbital is 5−7 eV, entirely consistent with the present work.[33,34] Therefore, we can now suggest that for oxide materials LDA + U with a U_p value of 7 eV will be suitable for first-principles calculations, even where experimental data are lacking, providing a predictive capability for the LDA + U approach.

dx.doi.org/10.1021/jp111167u |J. Phys. Chem. C 2011, 115, 4680–4687

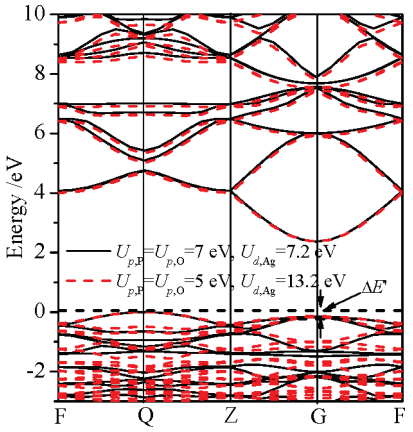

Figure 3. Energy band structure of Ag_3PO_4 calculated within the LDA + U_d + U_p approach. The Fermi level is set to the zero of energy. $\Delta E'$ is the energy difference of the VBM between Q and G points. Due to complete symmetry between spin-up and spin-down states, we only showed spin-up energy band structure.

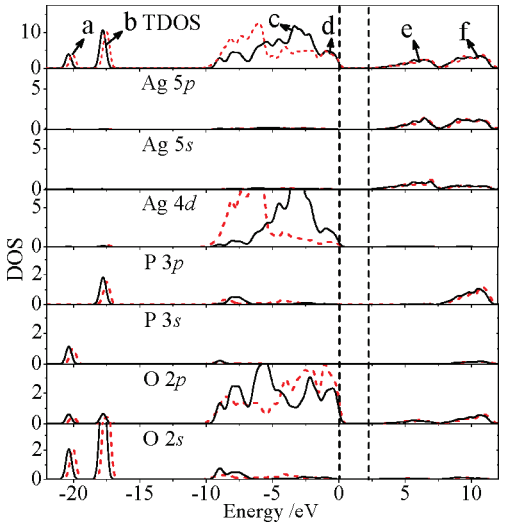

Figure 4. DOS of Ag_3PO_4 calculated within the LDA + U_d + U_p approach. The Fermi level is set to the zero of energy. Black solid lines denote $U_{p,P} = U_{p,O} = 7$ eV, $U_{d,Ag} = 7.2$ eV; red dotted lines denote $U_{p,P} = U_{p,O} = 5$ eV, $U_{d,Ag} = 13.2$ eV. Due to complete symmetry between spin-up and spin-down states, we only showed spin-up DOS.

In general, the calculations involving U_d and U_p show an upward shift of the CBM as well as a downward shift of VBM.[18] In other words, the U_d + U_p increases the splitting between occupied and empty energy levels since the correction is dependent on the occupancy of the orbitals. For a better understanding of the effect of U_d and U_p, we compared the energy band structure employing LDA + U_d + U_p, where $U_{p,P} = U_{p,O} = 5$ eV, $U_{d,Ag} = 13.2$ eV and $U_{p,P} = U_{p,O} = 7$ eV, $U_{d,Ag} = 7.2$ eV were taken. Figure 3 shows that the CB levels of Ag_3PO_4 calculated by the above two schemes of U parameters is fairly similar, and so is the top of the VB; however, the other part of the VB is obviously different from each other. From Figure 3, we can also see that it is an indirect band gap of 2.36 eV along the Q to G point. The direct band gap at the highly symmetric G point is 2.47 eV, which is slightly higher than 2.43 eV from the measurements for absorption spectrum.[9] The calculations within LDA + U_d and LDA + U_d + U_p approaches were employed to investigate the effect of the U parameter on the VBM along the Q direction to G ($\Delta E'$, see Figure 3). There is no obvious change of $\Delta E'$ at the energy level, so this further identifies that the material is an indirect band gap semiconductor. The indirect band gap and the direct band gap at the G point are energetically very close together, which also explains the features of the measured absorption spectrum (see Figure S1 in ref 9) as well as the very steep rise in photocurrent. For getting some information to interpret them, the corresponding partial DOS (PDOS) is presented in Figure 4. The root of the main difference of the VB is the Ag 4d PDOS. The Ag 4d orbital calculated by $U_{d,Ag} = 13.2$ eV is lower than that by $U_{d,Ag} = 7.2$ eV, in which the on-site Coulomb interaction (U_{d-d}) for Ag 4d states severely affects the energy band structures; however, the experimental data are not available.

To further clarify the complicated bonding character of the system, we presented the orbital information associated with the selected states (a, b, c, d, e, f) marked with ellipses in the DOS of Figure 4, as shown in Figure 5. The contour maps were constructed in the plane containing Ag, P, and O atoms. From the contour distribution, we can see the character of σ or π bonding states in the VB and the corresponding σ^* or π^* antibonding states in the CB. Figure 5(a) shows that there is an obvious directional σ bonding between the P and O atoms. Combined with the PDOS analysis, it can be concluded that the form of σ bonding states derives from the O p_σ states and P sp^3-hybridized states in the region of −21.2 to −19.2 eV. Geometries call for a sp^3 hybridization of the central P atom to form four σ bonds (from O p_z) in the PO_4 tetrahedron. Meanwhile, there is also a directional π bonding state from the hybridization between P sp^3 and O p_π states (from p_x and p_y orbitals perpendicular to the P−O bonds) in the region of −8.5 to −2.5 eV. The nonbonding states from the O 2s and Ag 4d states in the region of −18.1 to −17.0 eV and −6.2 to −0.5 eV are shown in Figure 5(b) and (c), respectively. Figure 5(d) shows that the top of the VB consists of the O $2p_\pi$ states where the hybridization with other states is almost negligible, leaving O $2p_\pi$ nonbonding states. The CB is decomposed into two main regions: the π^* antibonding in the lower-energy region (<7.7 eV) and σ^* antibonding in the higher-energy region (>7.7 eV). A significant feature of Ag_3PO_4 can be seen at the bottom of the CB where the Ag sp^3 hybridization states are dominantly located, as shown in Figure 5(e). However, the rest of the Ag sp^3 states are antibonding with the O $2p_\pi$ states, and the top of the CB is antibonding from the hybridization between P sp^3 and O $2p_\sigma$ states, as shown in Figure 5(f). A molecular-orbital bonding diagram, derived from the character of the states as discussed above, is presented in Figure 6.

Another measure of interest is the curvature of the parabolic portions of the bands near the CBM and VBM. The following simple relation equates the curvature of the bands to the effective mass of the electrons or holes[35]

$$m^* = \frac{\hbar^2}{2a} \quad (1)$$

where m^* is the effective mass of charge carrier and a is the coefficient of the second-order term in a quadratic fit of $E(k)$. Typical fitting results are plotted in Figure 7. The coefficient of the second-order term in a quadratic fit of $E(k)$ is 34.04(±0.22) for the bottom of the CB and −9.40(±0.21) for the top of the VB. Here, a large coefficient of the second-order term is corresponding to the low effective mass of the charge carrier, which implies a high mobility of charge carrier. From eq 1, we can

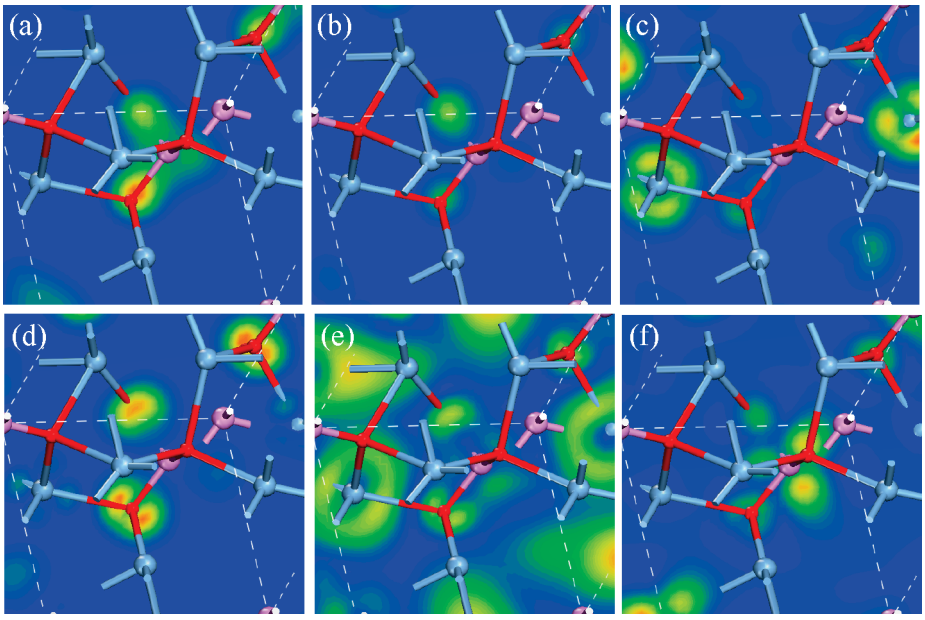

Figure 5. Charge density contour maps for various electronic states of Ag_3PO_4 (red, purple, and blue spheres represent O, P, and Ag atoms, respectively) corresponding to the selected energy peak (a, b, c, d, e, f) marked with ellipses in the DOS. The results are calculated within the LDA + U_d + U_p approach, where $U_{p,P}$ and $U_{p,O}$ are all 7 eV and $U_{d,Ag}$ is 7.2 eV.

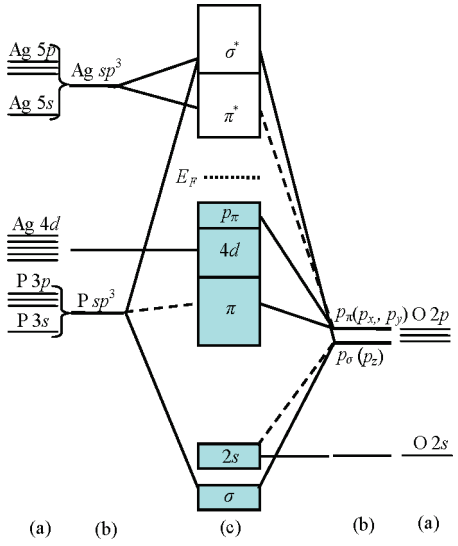

Figure 6. Molecular orbital bonding structure for Ag_3PO_4: (a) atomic levels, (b) hybridization orbitals, and (c) final interaction states. The thin-solid and dashed lines represent large and small contributions, respectively.

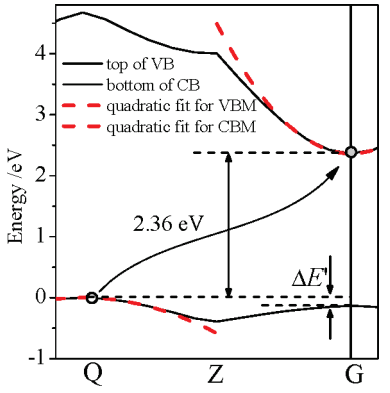

Figure 7. Plot of the two energy bands containing the CBM and VBM along Z from the Q to G point. The effective mass calculations are based on the quadratic fit of the red dashed curves. The minimum band gap is indirect with the CBM at G and the VBM at Q. The two energy bands are calculated within the LDA + U_d + U_p approach, where $U_{p,P}$ and $U_{p,O}$ are all 7 eV and $U_{d,Ag}$ is 7.2 eV. $\Delta E'$ is the energy difference of the VBM between the Q and G points.

figure out that the effective mass of electrons is far smaller than that of holes, which consequently results in a striking difference of the mobility between photoexcited electrons and holes. This is beneficial for decreasing the recombination of electron−hole pairs. Furthermore, the CB dispersion of Ag_3PO_4 is similar to anatase TiO_2 (see Figure S3 of the Supporting Information). In fact, the activity of d^{10} metal oxides and nitrides is associated with the CB of hybridized sp orbitals with large dispersion that are able to generate photoexcited electrons with high mobility.[7,30] This in turn is likely to suppress the recombination of electron−hole pairs and thus account for the high photooxidative activity.

The band edge energies of the CB could not be determined directly by electrochemical analysis. To give direct analysis, the band edge energies of the CB and VB of Ag_3PO_4 can be estimated from the absolute electronegativity of the atoms and the band gap of the semiconductors by eqs 2 and 3[36−38]

$$E_C = -(\chi(A)^a \cdot \chi(B)^b \cdot \chi(C)^c)^{1/(a+b+c)} + \frac{1}{2}E_g + E_0 \quad (2)$$

$$E_V = E_C + E_g \quad (3)$$

where $\chi(A)$, $\chi(B)$, and $\chi(C)$ are the absolute electronegativity of the atoms A, B, and C, respectively; E_C, E_V, and E_g are the band edge energies of the CB and the VB and the band gap of semiconductor, respectively; and E_0 is the scale factor relating the reference electrode redox level to the absolute vacuum scale

(AVS) ($E_0 = -4.5$ eV for a normal hydrogen electrode (NHE)). In fact, the electronegativity, χ, of a compound is the geometric mean of the electronegativities of the constituent atoms. Butler and Ginley had demonstrated that E_C values for oxide semiconductors calculated using eq 2 are in good agreement with the experimental values.[39] Here, we also calculated the band edge energies of the CB and VB of Ag_2O. For Ag_3PO_4 and Ag_2O, the geometric mean of the electronegativity χ is 5.96 and 5.29 eV, respectively. Thus, according to eq 2, the E_C of Ag_3PO_4 and Ag_2O could be calculated as 0.28 and −0.09 eV (vs NHE), respectively. In addition, the band gaps of Ag_3PO_4 and Ag_2O are 2.36 and 1.4 eV,[9,40] respectively. According to eq 3, we deduce that the E_V of Ag_3PO_4 and Ag_2O is 2.64 and 1.31 eV (vs NHE), respectively. Obviously, the VB top of Ag_3PO_4 is more positive than that of Ag_2O, which indicates that the oxidation of Ag_3PO_4 is stronger than that of Ag_2O. In addition, the oxidation potential of Ag_3PO_4 is slightly lower than that of anatase TiO_2 (2.70 eV) and monoclinic $BiVO_4$ (2.73 eV),[41] which may facilitate for the holes generated to react with OH^-, producing active ·OH radicals. This may be one reason for the strong oxidation of photoexcited holes. However, the driving force due to the difference between the potential of the VB of TiO_2 (or $BiVO_4$) and Ag_3PO_4 is not large enough to completely explain why the activation of Ag_3PO_4 is greatly higher than that of TiO_2 (or $BiVO_4$).[9] So it is reasonable to believe that there are some other reasons for its high activation.

3.3. Stability of Ag Vacancies and Defect Levels. As the Ag_3PO_4 oxidizes water automatically while simultaneously itself being reduced under visible-light irradiation, the yielding of Ag vacancies is indispensable.[9] To further get the origin of highly photocatalytic activation of Ag_3PO_4, the formation energies of Ag vacancies are calculated. A supercell consisting of a $2 \times 2 \times 2$ periodic repetition of the primitive unit cell is used. To introduce an isolated Ag vacancy, an interior Ag atom is removed from the supercell. The nearest and next-nearest atoms located within a radius of about 4.0 Å from defects are allowed to relax.

In fact, in thermodynamic equilibrium the concentration c of point defects is given by the expression $c = N_{site}N_{config}\exp(-E_f/kT)$.[42] Here, E_f is the defect formation energy, and lower E_f means a higher defect concentration c, which directly determines the physical and chemical behavior of Ag_3PO_4. In other words, defects with lower formation energies are more likely to form. The formation energy of a defect with charge state is defined as

$$E_f(D^q) = E_{tot}(D^q) - E_{tot}(\text{perfect}) + n_{Ag}\mu_{Ag} + q(E_F + E^q_{VBM}) \quad (4)$$

where $E_{tot}(D^q)$ is the total energy of a defective supercell with charge state q, and $E_{tot}(\text{perfect})$ is the total energy of the perfect supercell. Here n_{Ag} is the number of Ag atoms removed from the perfect supercell to introduce Ag vacancies. To succeed, a certain number of difficult problems had to be solved. First, the E^q_{VBM} value of a defective supercell is obtained from that of the perfect supercell and a difference ΔV in average potentials (V_{av}) between the perfect supercell and defective supercells as follows[43]

$$E^q_{VBM} = E^{perfect}_{VBM} + \Delta V \quad (5)$$

The first term of the right-hand side of eq 5 can be contained by $E^{perfect}_{VBM} = E_T(\text{perfect}; -1) - E_T(\text{perfect}; 0)$, where $E_T(\text{perfect}; 0)$ is the total energy of the neutral perfect supercell and $E_T(\text{perfect}; -1)$ is the total energy of the −1 charged perfect supercell corresponding to the situation that one electron is removed from the VBM of the neutral perfect supercell.

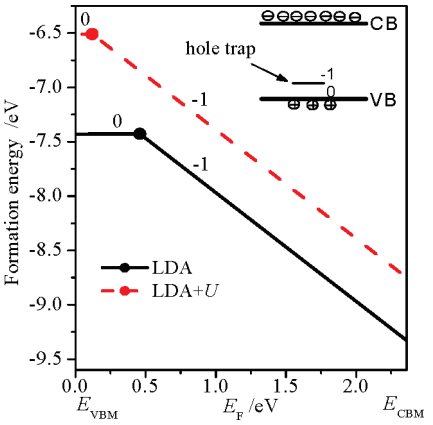

Figure 8. Formation energies of Ag vacancies as a function of the Fermi level, under the Ag-rich growth conditions. The zero energy of E_F corresponds to the VBM, while the value, 2.36 eV, indicates the CBM using the experimental E_g value. Red dashed lines denote $U_{p,P} = U_{p,O} = 7$ eV and $U_{d,Ag} = 7.2$ eV.

Figure 8 shows the formation energies of the Ag vacancies in Ag_3PO_4 as a function of the Fermi level E_F under the Ag-rich growth conditions. Filled circles denote the position of thermodynamic transition levels $\varepsilon(0/-1)$, which is defined as the Fermi-level position where charge states 0 and −1 have equal energy. The thermodynamic transition levels $\varepsilon(0/-1)$ are usually called the thermal ionization energy or the acceptor ionization energy E_A. As the name implies, the level would be observed in experiments where the final charge state can fully relax to its equilibrium configuration after the transition. From Figure 8, we see that when E_F is near the VBM $E_f(V_{Ag}, 0)$ and $E_f(V_{Ag}, -1)$ are both negative, so the Ag vacancies will form spontaneously. The lower E_f means a high defect concentration of Ag vacancies in Ag_3PO_4. In fact, Ag vacancies behave as shallow acceptors in Ag_3PO_4 (notice the dependence on E_F in Figure 8; a decrease of formation energy with E_F is indicative of acceptors).[42]

Its lowest defect transition level is $\varepsilon_{V_{Ag}}(0/-1) = E_{VBM} + 0.46$ eV inside the band gap within the LDA approach, so it is ionized only when E_F is below this position. Similarly, within the LDA + U approach ($U_{p,P} = U_{p,O} = 7$ eV, $U_{d,Ag} = 7.2$ eV), $\varepsilon_{V_{Ag}}(0/-1)$ is $E_{VBM} + 0.12$ eV. Hence, V_{Ag} have two charge states, 0 and −1. It is clear that the acceptor levels of V_{Ag} in Ag_3PO_4 are shallow because the outer electrons of Ag atoms are more weakly bound than those of P atoms. The exciting light creates electron−hole pairs. The holes can be trapped at V_{Ag}^{-1} centers, turning them into V_{Ag}^{0}. Using the definition of the thermal ionization energy E_A,[42] the equilibrium configuration of the $V_{Ag}^{0} + e$ state (where e is an electron at the bottom of the CB) is $E_g - E_A$ higher than the equilibrium configuration of V_{Ag}^{-1}, where E_g is the band gap. In fact, VBM at the Q point is slight higher than that at the G point, so the relaxation energy E_{rel} between Q and G points is very small. It is well-known that the optical ionization energy, E_A^{opt}, is defined as $E_A + E_{rel}$.[42] As a result, the E_A^{opt} should be slightly larger than the thermal ionization energy E_A by an amount E_{rel}. It is clear that the defect levels in the band gap of Ag_3PO_4 will act as capture traps for photoexcited holes, resulting in improvement in photocatalytic activation under visible-light irradiation. On the other hand, due to the strong P−O covalence, PO_4^{3-} ions are difficult to form oxygen vacancies which are

dx.doi.org/10.1021/jp111167u |J. Phys. Chem. C 2011, 115, 4680–4687

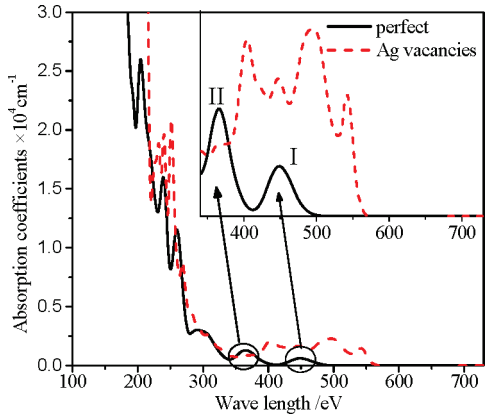

Figure 9. Calculated total absorption coefficient spectra of Ag_3PO_4. The inset shows enlarged absorption coefficient spectra in the range from 340 to 730 nm.

considered as the recombination centers in TiO_2 or other metal oxide and composite metal oxide photocatalysts. In addition, PO_4^{3-} ions on the surface of Ag_3PO_4 may also play the same part as they do in the TiO_2 surface, such as the strong bonding ability with H_2O. These benefits of PO_4^{3-} ions in the structure may result in its photocatalytic superiority, which is also found for $BiPO_4$ in our previous study.[44]

3.4. Optical Absorption. The study of the optical properties of Ag_3PO_4 is very necessary in the visible-light photocatalytic realm. The absorption coefficient indicates the fraction of energy lost by the electromagnetic wave when it passes through a unit thickness of the material, and it is proportional to the rate of Joule heat produced in the sample. We obtain the spectra by calculating the imaginary part of the complex dielectric function using eq 1 of ref 19 within the spin-polarized LDA + U approach. The allowed transitions are determined by the nonzero matrix elements of the position operator. The optical calculations are performed using the "polycrystalline" polarization where the E field vector is an isotropic average over all directions. In the calculations of the spectra, we used a small smearing of 0.1 eV to better distinguish the absorption peaks.

Figure 9 shows the optical absorption spectrum for the perfect Ag_3PO_4. It is clear that the absorption band edge of perfect Ag_3PO_4 corresponding to the largest wavelength is below 500 nm. It is noted that there are two peaks (I and II) showing maximum intensities at wavelengths about 450 and 378 nm, respectively. Peak I (the range of indigo color) corresponds to photo transition energies from the VBM to the CB, namely, electron transfer from O 2p to Ag 5s orbitals under visible-light irradiation. This denotes that Ag_3PO_4 is a visible-light semiconductor photocatalyst. However, the absorption intensity of perfect Ag_3PO_4 is weak in the visible-light range due to large dispersion of the hybridized sp orbitals. So, they are not enough to contribute to the highly photocatalytic activity of Ag_3PO_4. In addition, we also calculated the optical absorption spectrum of Ag vacancies' systems, which are obviously different from that of perfect Ag_3PO_4 in the visible-light region. It is interesting that Ag vacancies induce the increasing optical absorption range in the visible-light region (about 560 nm), and the absorption intensity of Ag_3PO_4 with Ag vacancies greatly exceeds that of the perfect Ag_3PO_4 in the long-wavelength range, corresponding to a photo transition energy of about 2.22 eV from the defect levels in the band gap to the CB. So, the defect levels in the band gap of Ag_3PO_4 will play a significant role in increasing the optical absorbance in the visible-light region.

4. CONCLUSIONS

In summary, the calculated results may help us understand the origin of photocatalytic activation of Ag_3PO_4 using first-principles DFT incorporating the LDA + U formalism. The results show that Ag_3PO_4 has an indirect band gap and a strong oxidation of photoexcited holes in the VB, and the mobility of the electrons is fairly higher than that of the holes, which facilitates the separation of electron−hole pairs partly due to the form of the delocalized π^* antibonding states in the CB. In addition, the inductive effect of PO_4^{3-} facilitates the e^-/h^+ separation, which plays an important role in its excellent photocatalytic activity. Our results suggest that the defect states of Ag vacancies would act as capture traps for photoexcited holes, which subsequently promotes the separation of electron−hole pairs excited under visible-light irradiation.

■ ASSOCIATED CONTENT

Supporting Information. (1) The difference charge density contour maps for Ag_3PO_4, (2) the energy band structure and DOS of Ag_3PO_4 calculated within the LDA approach, and (3) a plot of the two energy bands of TiO_2 containing the bottom of the CB and the top of the VB along the G direction from M to Z point. This material is available free of charge via the Internet at http://pubs.acs.org.

■ AUTHOR INFORMATION

Corresponding Author

*E-mail: zhuyf@mail.tsinghua.edu.cn. Tel.: (+86)10-6278-3586. Fax: (+86)10-6278-7601.

■ ACKNOWLEDGMENT

This work was supported by the National Natural Science Foundation of China (20925725 and 50972070) and the National Basic Research Program of China (2007CB613303). The authors gratefully acknowledge Professor Lin Miao for valuable discussions on this topic.

■ REFERENCES

(1) Zou, Z. G.; Ye, J. H.; Sayama, K.; Arakawa, H. *Nature* **2001**, *414*, 625.
(2) Kudo, A.; Ueda, K.; Kato, H.; Mikami, I. *Catal. Lett.* **1998**, *53*, 229.
(3) Kohtani, S.; Tomohiro, M.; Tokumura, K.; Nakagaki, R. *Appl. Catal., B: Environ.* **2005**, *58*, 265.
(4) Fu, H. B.; Zhang, S. C.; Xu, T. G.; Zhu, Y. F.; Chen, J. M. *Environ. Sci. Technol.* **2008**, *42*, 2085.
(5) Shang, M.; Wang, W. Z.; Zhang, L.; Xu, H. L. *Mater. Chem. Phys.* **2010**, *120*, 155.
(6) Wei, W.; Dai, Y.; Yang, K. S.; Guo, M.; Huang, B. B. *J. Phys. Chem. C* **2008**, *112*, 15915.
(7) Maeda, K.; Domen, K. *Chem. Mater.* **2010**, *22*, 612.
(8) Ouyang, S. X.; Li, Z. S.; Ouyang, Z.; Yu, T.; Ye, J. H.; Zou, Z. G. *J. Phys. Chem. C* **2008**, *112*, 3134.
(9) Yi, Z. G.; Ye, J. H.; Kikugawa, N.; Kako, T.; Ouyang, S. X.; Stuart-Williams, H.; Yang, H.; Cao, J. Y.; Luo, W. J.; Li, Z. S.; Liu, Y.; Withers, R. L. *Nat. Mater.* **2010**, *9*, 559.

(10) Ng, H. N.; Calvo, C.; Faggiani, R. *Acta Crystallogr. B* **1978**, *34*, 898.
(11) Masse, R.; Tordjman, I.; Durif, A. *Z. Kristallogr.* **1976**, *114*, 76.
(12) Kohn, W.; Sham, L. J. *Phys. Rev.* **1965**, *140*, A1133.
(13) Perdew, J. P.; Burke, K.; Ernzerhof, M. *Phys. Rev. Lett.* **1996**, *77*, 3865.
(14) Kilic, C.; Zunger, A. *Phys. Rev. Lett.* **2002**, *88*, 095501.
(15) Dudarev, S. L.; Botton, G. A.; Savrasov, S. Y.; Humphreys, C. J.; Sutton, A. P. *Phys. Rev. B* **1998**, *57*, 1505.
(16) Walsh, A.; DaSilva, J. L. F.; Wei, S.-H. *Phys. Rev. Lett.* **2008**, *100*, 256401.
(17) Lathiotakis, N. N.; Andriotis, A. N.; Menon, M. *Phys. Rev. B* **2008**, *78*, 193311.
(18) Park, S. G.; Magyari-Köpe, B.; Nishi, Y. *Phys. Rev. B* **2010**, *82*, 115109.
(19) Sheetz, R. M.; Ponomareva, I.; Richter, E.; Andriotis, A. N.; Menon, M. *Phys. Rev. B* **2009**, *80*, 195314.
(20) Volnianska, O.; Boguslawski, P.; Kaczkowski, J.; Jakubas, P.; Jezierski, A.; Kaminska, E. *Phys. Rev. B* **2009**, *80*, 245212.
(21) Segall, M. D.; Lindan, P. L. D.; Probert, M. J.; Pickard, C. J.; Hasnip, P. J.; Clark, S. J.; Payne, M. C. *J. Phys.: Condens. Matter* **2002**, *14*, 2717.
(22) Vanderbilt, D. *Phys. Rev. B* **1990**, *41*, 7892.
(23) Monkhorst, H. J.; Pack, J. D. *Phys. Rev. B* **1976**, *13*, 5188.
(24) Sanchez-Portal, D.; Artacho, E.; Soler, J. M. *Solid State Commun.* **1995**, *95*, 685.
(25) Segall, M. D.; Shah, R.; Pickard, C. J.; Payne, M. C. *Phys. Rev. B* **1996**, *54*, 16317.
(26) Pei, F.; Wu, S.; Wang, G.; Xu, M.; Wang, S. Y.; Chen, L. Y.; Jia, Y. *J. Korean Phys. Soc.* **2009**, *55*, 1243.
(27) Ma, X. G.; Jiang, J. J.; Bie, S. W.; Miao, L.; Zhang, C. K.; Wang, Z. Y. *Intermetallics* **2010**, *18*, 2399.
(28) Zaghiba, K.; Julien, C. M. *J. Power Sources* **2005**, *142*, 279.
(29) Sato, J.; Kobayashi, H.; Inoue, Y. *J. Phys. Chem. B* **2003**, *107*, 7970.
(30) Inoue, Y. *Energy Environ. Sci.* **2009**, *2*, 364.
(31) Nolan, M.; Watson, G. W. *J. Chem. Phys.* **2006**, *125*, 144701.
(32) Nolan, M.; Watson, G. W. *Surf. Sci.* **2005**, *586*, 25.
(33) Ghijsen, J.; Tjeng, L. H.; van Elp, J.; Eskes, H.; Westerink, J.; Sawatzky, G. A.; Czyzyk, M. T. *Phys. Rev. B* **1988**, *38*, 11322.
(34) Knotek, M. L.; Fiebelman, P. J. *Phys. Rev. Lett.* **1978**, *40*, 964.
(35) Thulin, L.; Guerra, J. *Phys. Rev. B* **2008**, *77*, 195112.
(36) Xu, Y.; Schoonen, M. A. A. *Am. Mineral.* **2000**, *85*, 543.
(37) Pearson, R. G. *Inorg. Chem.* **1988**, *27*, 734.
(38) Lv, J.; Kako, T.; Li, Z. S.; Zou, Z. G.; Ye, J. H. *J. Phys. Chem. C* **2010**, *114*, 6157.
(39) Butler, M. A.; Ginley, D. S. *J. Electrochem. Soc.* **1978**, *125*, 228.
(40) Yahia, K. Z. *Eng. Technol.* **2008**, *26*, 570.
(41) Li, H. B.; Liu, G. C.; Duan, X. C. *Mater. Chem. Phys.* **2009**, *115*, 9.
(42) Van de Walle, C. G.; Neugebauer, J. *J. Appl. Phys.* **2004**, *95*, 3851.
(43) Ma, X. G.; Jiang, J. J.; Liang, P.; Wang, J. *Trans. Nonferrous Met. Soc. China* **2007**, *17*, s50.
(44) Pan, C. S.; Zhu, Y. F. *Environ. Sci. Technol.* **2010**, *44*, 5570.